Analysis of the Intrinsic Mid-Infrared L-band to Optical Flux Ratios In Spectral Synthesis Models of Composite Stellar Populations

Duho Kim[1], Rolf A. Jansen[1,2] & Rogier A. Windhorst[1,2]
[1]School of Earth and Space Exploration, Arizona State University, P.O. Box 871404, Tempe, AZ 85287-1404, USA
[2]Department of Physics, Arizona State University, Tempe, AZ 85287-1504, USA

[#143.14]

Abstract

We analyze the intrinsic flux ratios of simple and composite stellar populations for various visible to near-infrared (NIR) filters with respect to ~ 3.5μm (*L*-band) and their dependence on metallicity, star-formation history, and effective mean age. This study is motivated by the fact that light from galaxies is attenuated by dust via scattering and absorption, where different sightlines suffer various amounts of extinction across the face of a galaxy. Ignoring the effects of extinction would therefore, lead to incorrect results. Tamura et al. (2009) developed an approximate method, dubbed the "β_V" method, which corrects for dust extinction on a pixel by pixel basis, by comparing the observed and empirical estimate of the intrinsic flux ratios of optical and 3.5μm broadband data. Here, we aim to validate and test the limits of the "β_V" method for various filters spanning the visible through mid-infrared (MIR) wavelength range with extensive modeling to test their assumptions for the intrinsic flux ratios for a wide variety of simple and composite stellar populations. We build spectral energy distribution (SED) models of simple stellar population (SSP), by adopting Starburst99 (SB99; Leitherer et al. 1999) and BC03 (Bruzual & Charlot 2003) models for young (<9Myr) and old (>100Myr) stellar populations, respectively, and linear combinations of these for intermediate ages. We then construct composite stellar population (CSP) SEDs by combining SSP SEDs for various realistic star-formation histories (SFHs). Filter response curves for large number of visible through mid-infrared filters commonly used for *HST* imaging surveys and for current (*WISE*, *Spitzer* IRAC) and near-future (e.g., *JWST*/NIRCam, *WFIRST*) are folded with each model SED to obtain intrinsic flux ratios ($\beta_{\lambda,0}$). We present these $\beta_{\lambda,0}$ as a function of the age and metallicity of stellar populations, and discuss the effect of various SFHs. We also present ranges of $\beta_{\lambda,0}$ values expected for different types of galaxies.

Combining SB99 & BC03

We built SSP SEDs by adopting the Geneva track of SB99 for young ages and the Padova track of BC03 for old ages. We scrutinized absolute flux differences between SB99 and BC03 in percentages (see Figure 1), and interpolate between SB99 and BC03 SEDs in the intermediate ages (see Table 1).

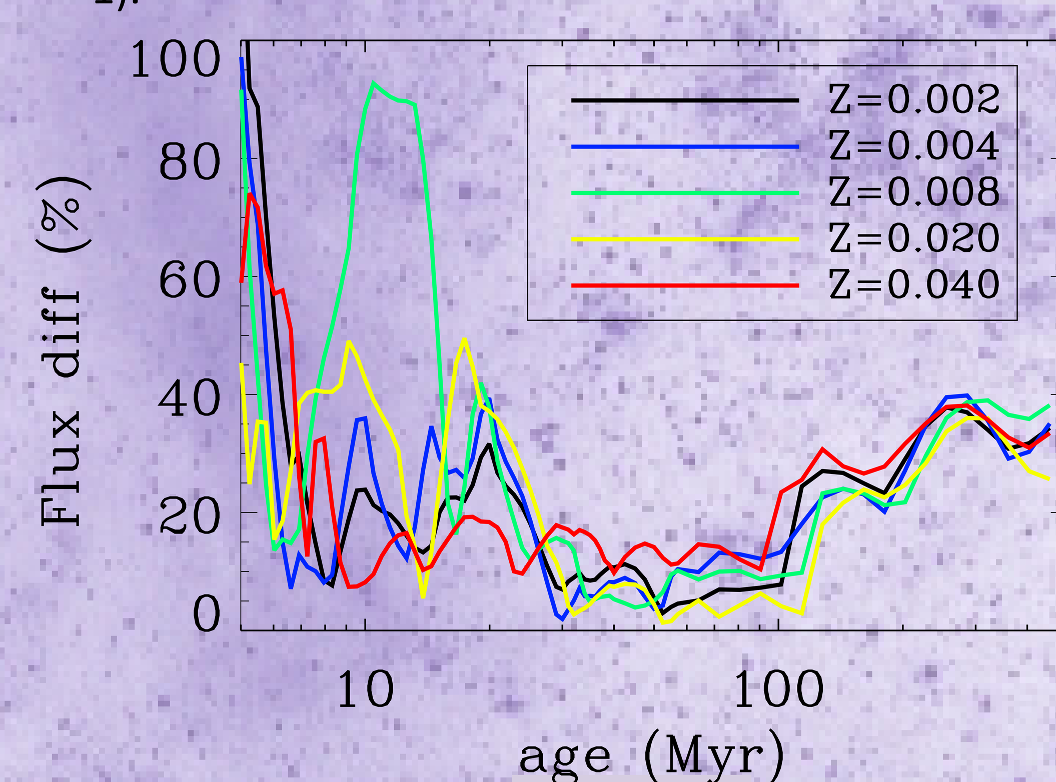

Figure 1

Z	Age range
0.002	30-100 Myr
0.004	25-55 Myr
0.008	35-75 Myr
0.02	30-100 Myr
0.04	9-90 Myr

Table 1

$\beta_{\lambda,0}$ values for SSP and CSP

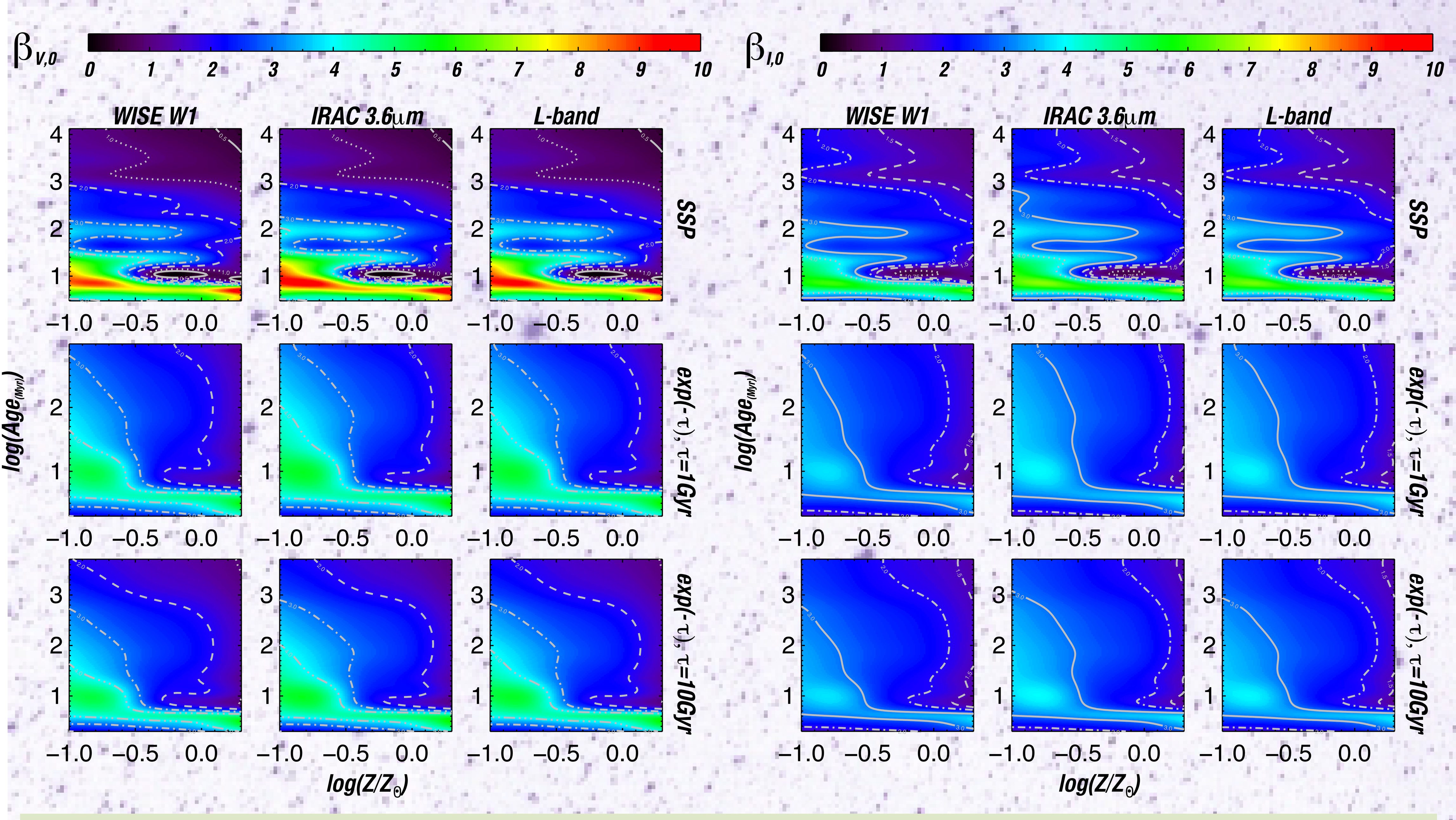

Composite Stellar Population (CSP) Modeling

We generated CSP SEDs by convolving SSP SEDs as a function of SFH (ψ(t)).

$$F_{\lambda,\mathrm{CSP}}(t', Z') = \sum_{t=t_0}^{t'} F_{\lambda,\mathrm{SSP}}(t, Z(t, Z'))\psi(t)\delta t$$

Intrinsic flux ratios between visible to NIR and MIR ($\beta_{\lambda,0}$)

We can obtain extinction value (A_V) simply using visible to NIR and MIR observations, if we know intrinsic flux ratio of those.

$$\beta_{\lambda,0} = \frac{f_{\lambda,0}}{f_{3.6\mu m}} \qquad A_V = m_V - [-2.5\log(\beta_{V,0} \times f_{3.6\mu m}) - V_{\mathrm{ZP}}]$$

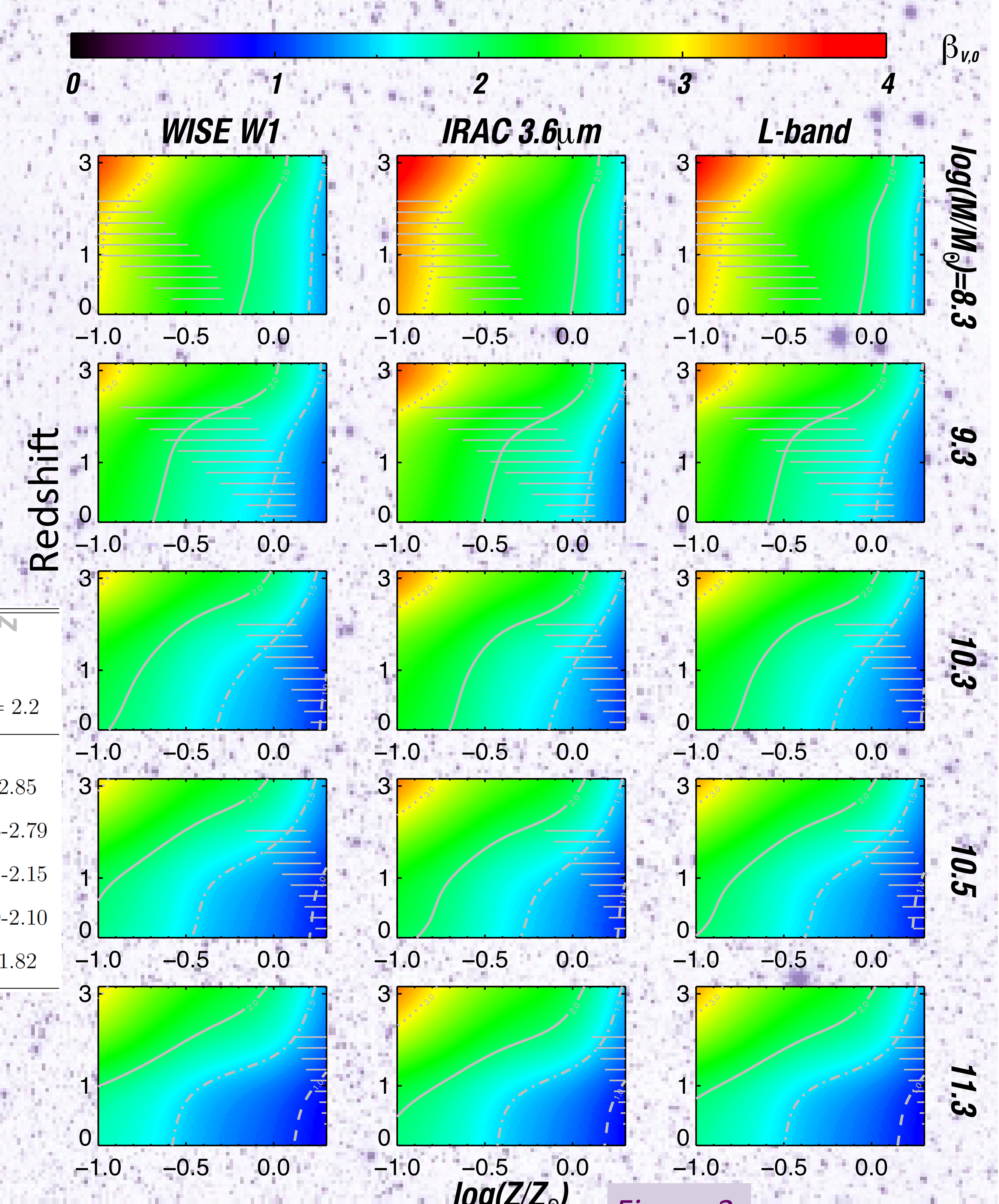

Figure 3

$\beta_{\lambda,0}$ values for Star-forming Galaxies (SFGs)

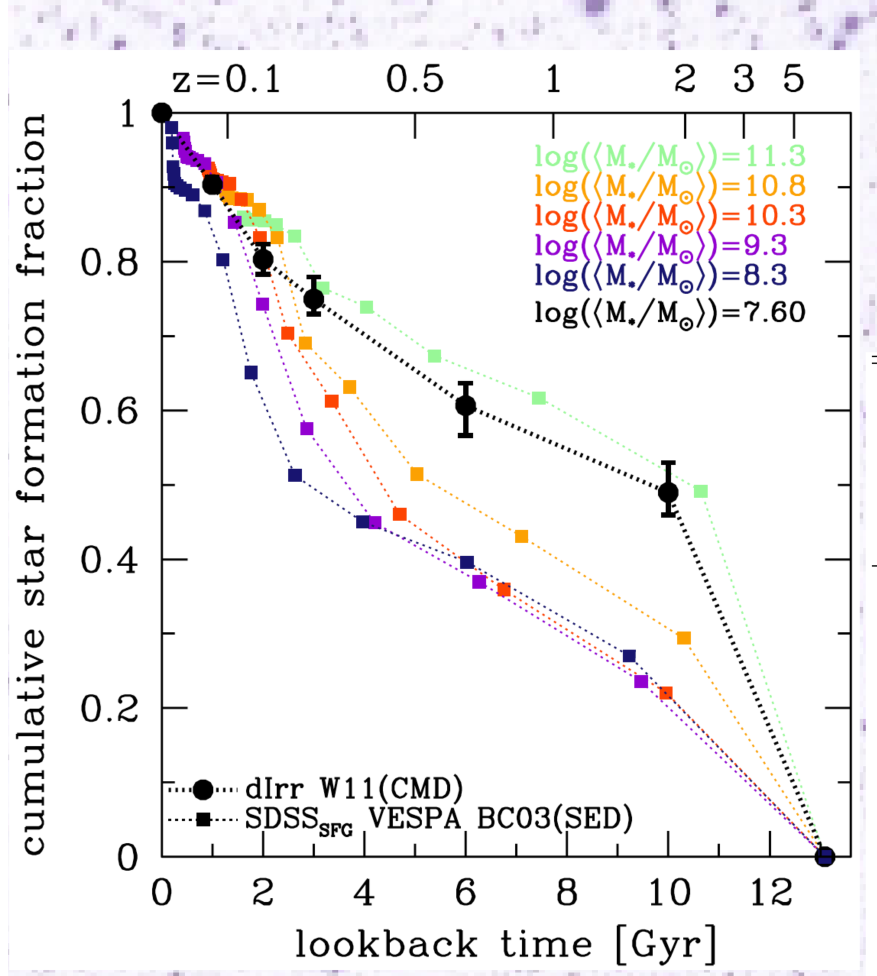

Figure 2

We have used SFH result (Figure 2) of SDSS SFGs from Leitner 2012 and generated $\beta_{\lambda,0}$ values (Figure 3). In order to find reasonable metallicity ranges for each mass of galaxies, we adopted the result of mass metallicity evolution from Maiolino et al. 2008 (see the horizontal lines in Figure 3). Expected $\beta_{\lambda,0}$ values for different mass of galaxies as a function of redshifts are presented in Table 2.

Mass Range ($M_\odot$)	$\beta_{V,0}$			$\beta_{I,0}$		
	$z=0.07$	$z=0.7$	$z=2.2$	$z=0.07$	$z=0.7$	$z=2.2$
$10^8 - 10^{8.5}$	2.05-2.24	2.14-2.76	$\gtrsim$ 2.89	2.22-2.39	2.28-2.80	$\gtrsim$ 2.85
$10^9 - 10^{9.5}$	1.08-1.08	1.60-1.73	1.96-2.66	1.41-1.41	1.93-2.08	2.16-2.79
$10^{10} - 10^{10.5}$	$\lesssim$ 1.04	0.98-1.23	1.55-1.89	$\lesssim$ 1.43	1.34-1.62	1.81-2.15
$10^{10.5} - 10^{11}$	$\lesssim$ 0.93	$\lesssim$ 1.09	1.43-1.84	$\lesssim$ 1.35	$\lesssim$ 1.50	1.69-2.10
$10^{11} - 10^{11.5}$	$\lesssim$ 0.83	$\lesssim$ 0.9	$\lesssim$ 1.57	$\lesssim$ 1.28	$\lesssim$ 1.32	$\lesssim$ 1.82

Table 2

References

Bruzual, G., & Charlot, S. 2003, MNRAS, 344, 1000
Leitherer, C., Schaerer, D., Goldader, J. D., et al. 1999, ApJS, 123, 3
Leitner, S. N. 2012, ApJ, 745, 149
Maiolino, R., Nagao, T., Grazian, A., et al. 2008, A&A, 488, 463
Tamura, K., Jansen, R. A., & Windhorst, R. A. 2009, AJ, 138, 1634
Tamura, K., Jansen, R. A., Eskridge, P. B., Cohen, S. H., & Windhorst, R. A. 2010, AJ, 139, 2557

Acknowledgements

This work was funded by NASA/ADAP grant NNX12AE47G (PI: R. A. Jansen)